J. Water Environ. Nanotechnol., 9(2): 137-148 Spring 2024

ORIGINAL RESEARCH PAPER

Synthesis of ZnO Nanostructures with Different Morphologies on Biochar Support for Photocatalytic Degradation of Organic Dye

Maryam Fayazi*

Department of Environment, Institute of Science and High Technology and Environmental Science, Graduate University of Advanced Technology, Kerman, Iran

Received: 2023-11-20 Accepted: 2024-01-20 Published: 2024-05-12

ABSTRACT

In the present study, different morphologies (viz., spherical and nanorod) of zinc oxide (ZnO) were successfully deposited on the biochar support material via a simple hydrothermal approach. The biochar utilized in this research was obtained through the pyrolysis process of pistachio residues. Characterization of the prepared ZnO/biochar nanocomposites was carried out using FT-IR, XRD, DRS, EDS, and SEM analyses. DRS data analysis revealed that the band gap energies of the fabricated nanocomposites were measured to be 2.98 eV and 3.08 eV for the spherical ZnO/biochar and nanorod ZnO/biochar, respectively. Under visible light irradiations, the prepared photocatalysts were assessed for their photocatalytic abilities in the degradation of methylene blue (MB) dye. The degradation of MB on ZnO/biochar catalysts demonstrates a strong correlation with a pseudo-first-order kinetic model. Besides, the suggested photocatalyst substance indicated good reusability, retaining its performance for at least five cycles. The utilization of low-expense biochar support in conjunction with nanosized ZnO nanostructures presents a promising idea to achieve efficient photocatalysts for the degradation of organic pollutants.

Keywords: *Biochar, Spherical ZnO, Nanoroad ZnO, Photocatalytic activity, Methylene blue*

How to cite this article

Fayazi M., Synthesis of ZnO Nanostructures with Different Morphologies on Biochar Support for Photocatalytic Degradation of Organic Dye. J. Water Environ. Nanotechnol., 2024; 9(2): 137-148. DOI: 10.22090/jwent.2024.02.02

INTRODUCTION

The treatment of toxic and non-biodegradable organic contaminants, such as synthetic dyes, in water bodies necessitates the development of effective and sustainable technologies [1, 2]. To date, various protocols have been employed for the treatment of dye-containing wastewater including biological methods, coagulation/flocculation, advanced oxidation process, ion exchange, photocatalysis, and different adsorptive strategies [3, 4]. The photocatalysis approach offers a promising solution for the treatment of organic pollutants in environmental waters owing to its powerful oxidation capabilities, cost-effectiveness, mild operation conditions, and eco-friendly nature [5-7].

Zinc oxide (ZnO) is widely utilized as a photocatalyst because it possesses comparable band gap energy and favorable band gap positions in comparison to titanium dioxide (TiO_2) as the most used photocatalyst [8, 9]. From this point of view, extensive research has been conducted on ZnO for its ability to remove organic contaminants [10, 11] and microbial disinfection [12, 13]. The absorption of photons with energy equal to or higher than its band gap by ZnO leads to the creation of e^-/h^+ pairs, which then trigger redox reactions at the surface of the photocatalyst [14, 15]. The formation of hydroxyl radicals ($OH^\bullet$) occurs when the holes interact with H_2O molecules or OH^- ions at the surface of the ZnO photocatalyst through an oxidative reaction [16, 17]. In addition,

* Corresponding Authors Email: *maryam.fayazi@yahoo.com; m.fayazi@kgut.ac.ir*

the generated electrons can react with O_2 molecules and produce superoxide radicals ($O_2^{\bullet-}$) via a reductive process. The non-selective $OH^{\bullet}$ radicals, known for their high reactivity, cause damage to the structures of most organic compounds [18]. The wide optical band gap of ZnO, which is around 3.37 eV, imposes a constraint on its ability to absorb the visible portion of the solar spectrum [19]. Moreover, the rapid recombination of photo-generated charge carriers hinders the high photocatalytic ability of ZnO photocatalyst [20, 21]. The use of nonmetallic elements such as carbon, nitrogen, and sulfur has gotten a lot of attention for the improvement of photocatalytic operation of ZnO [22, 23]. Deposition of ZnO particles on porous carbonaceous materials can enhance degradation performance by facilitating both photo-induced electron transfer and adsorption of organic pollutants [24]. Activated carbon (AC) has been extensively utilized as a support for photocatalysts due to its simple fabrication, chemical constancy, porous structure with a significant surface area, and environmental friendliness [25]. Recently, biochar support has attracted considerable interest in water treatment [26]. The use of low-cost resources, particularly agricultural waste is the main advantage in the production of biochar material. This strategy offers a solution to agricultural waste disposal limitations and facilitates the conversion of waste substances into useful carbon material [27].

Herein, we focus on the fabrication of novel nanocomposite materials to make effective visible active photocatalysts by the combination of ZnO particles and agricultural waste-derived biochar. To reach this goal, firstly the pistachio residues were used as raw and available substances to fabricate the porous biochar via the pyrolysis process. After the hydrothermal treatment, various morphologies (spherical and road) of ZnO nanoparticles were immobilized onto the surface of biochar support, and composites (spherical ZnO/biochar and nanorod ZnO/biochar) were fabricated. The prepared ZnO-biochar nanocomposites were well characterized using different techniques including Fourier transform infrared spectroscopy (FT-IR), X-ray diffraction (XRD), UV-vis diffuse reflectance spectroscopy (DRS), scanning electron microscopy (SEM) and electron dispersive spectroscopy (EDS) elemental mapping. The photocatalytic performances of ZnO/biochar nanocatalysts were explored using the photodegradation of methylene blue (MB) as a target dye contaminant in an aqueous solution. Our investigation proposes a convenient and inexpensive technique to facilitate the practical use of ZnO photocatalyst.

EXPERIMENTAL

Chemicals and materials:

Zinc chloride ($ZnCl_2$), MB ($C_{16}H_{18}N_3SCl.3H_2O$), and ammonia solution (NH_4OH) were supplied from Merck (Germany) and used without any purification. In all synthesis and photocatalytic experiments, ultra-pure water was used. Pistachio samples were acquired from the Sirjan city (Kerman Province) of Iran.

Instrumentation:

MB residual concentrations and DRS data were obtained on a Varian spectrophotometer (Cary 5000). The morphologies of the prepared ZnO/biochar photocatalysts were evaluated with an MIRA3 LM TESCAN microscope equipped with an EDS system. The XRD patterns of biochar and ZnO/biochar nanocomposites were recorded on a powder XRD instrument (Malvern-PANalytical, Empyean 2012). Fourier transform infrared spectroscopy (FT-IR) spectra were recorded using a Perkin Elmer FT-IR system.

Preparation of ZnO/biochar nanocomposites:

The preparation of biochar support was carried out according to a method reported previously [28]. Firstly, the raw pistachio shells were dried at 110 °C in an oven to eliminate the moisture content. The dried shells were ground and put in 50 mL porcelain crucibles and then covered with lids. The crucible was subjected to a furnace to pyrolysis the biomass. The furnace was supplied with N_2 for 1 h at a rate of 50 mL min^{-1} to evacuate O_2. The powdered sample was pyrolyzed at 900 °C for 4 h with a heating rate of 10 °C min^{-1}. After cooling the furnace, the obtained biochar was collected, ground into powder, and stored in a desiccator to avoid moisture adsorption.

The ZnO-biochar nanocomposites with different morphologies were formed with the hydrothermal method according to the following procedures. In a typical procedure, 0.5 g of biochar sample was dispersed in 50 mL of deionized water under ultra-sonication for 15 min. Then, 0.68 g of $ZnCl_2$ was added to the above mixture under magnetic stirring for the next 15 min. Then, NH_4OH solution was added dropwise into the

obtained mixture to reach the pH value of mixture 9.0. After stirring for 1 h, the mixture was sealed into a Teflon-lined stainless autoclave (75 mL). The autoclave was sealed and maintained at 150 °C for 4 h for hydrothermal treatment. After cooling to room temperature, the precipitate was leached and rinsed with water 3 times and dried at 50 °C overnight. To achieve the spherical ZnO/biochar sample, the obtained processor was annealed at 400 °C for 4 h. The nanorod ZnO/biochar sample was similarly prepared except that the pH of the mixture solution was adjusted to 12.0 by NH_4OH solution. Scheme 1 shows a diagrammatic representation of the synthesized photocatalysts. According to literature reposted by Kumaresan et al. [29], the pH of precursor solution affects the morphology of ZnO particles. The adsorption of hydroxyl ions (OH^-) onto certain crystal facets can inhibit growth perpendicular to those surfaces. The combination of anisotropic growth kinetics and selective adsorption of OH^- ions ultimately causes one-dimensional growth and the formation of ZnO nanorods under higher pH conditions [30].

Photocatalytic degradation of MB:

The photocatalytic potency of spherical ZnO/biochar and nanorod ZnO/biochar was explored by evaluating the photodegradation of MB under visible light irradiation. A tubular reactor (with 50 mL volume) was used for the degradation studies. The reactor was illuminated using a 500-W high-pressure xenon lamp equipped with a UV cutoff filter, which provided visible light in the wavelength range from 400 nm to 800 nm. To get the adsorption-desorption equilibrium, the MB solution was stirred with 10 mg of the prepared photocatalysts in the dark for 20 min. Visible light irradiation was then applied to the stirred aqueous dye solution to initiate the photocatalytic reaction. The residual MB concentration was monitored using a spectrophotometer at regular 10-minute intervals during the experiment cycle time (2 h). The equation used to estimate the degradation yield of dye can be expressed as follows [31]:

$$\text{Degradation yield} = \frac{(C_0 - C_t)}{C_0} \times 100 \quad (1)$$

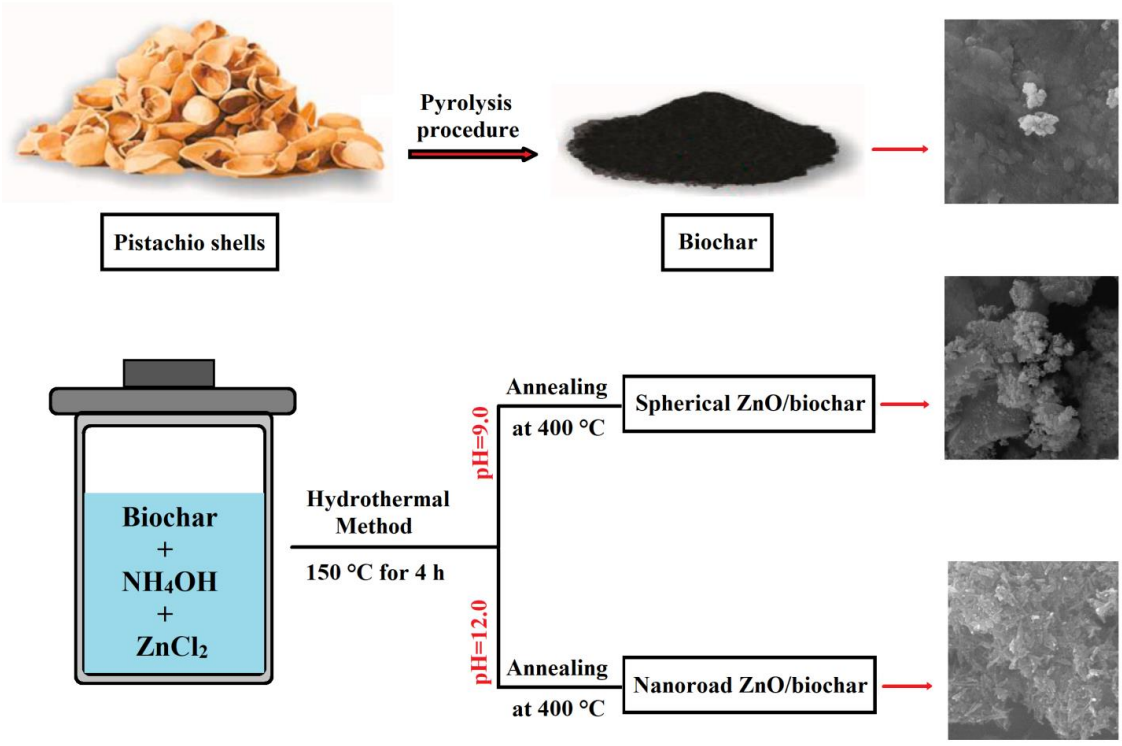

Scheme 1. Schematic presentation of steps involved in the fabrication of ZnO/biochar photocatalysts.

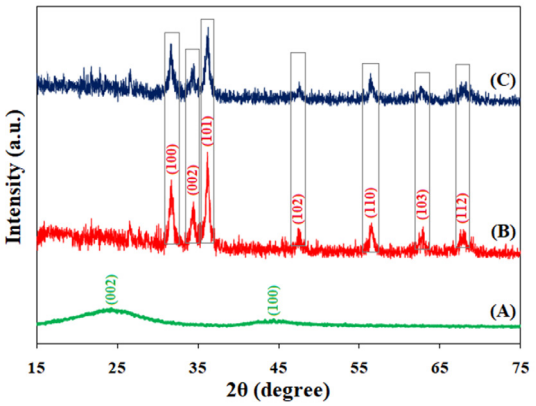

Fig. 1. XRD patterns of (A) biochar, (B) nanorod ZnO/biochar, and (C) spherical ZnO/biochar.

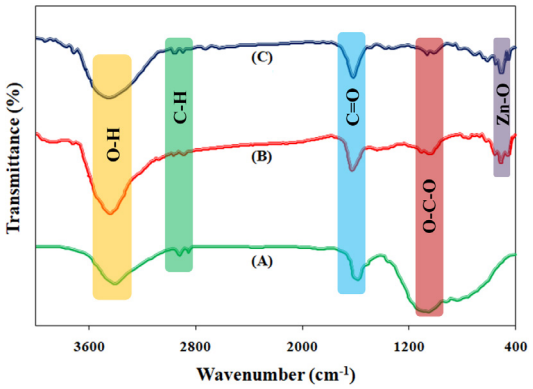

Fig. 2. FT-IR spectra of (A) biochar, (B) nanorod ZnO/biochar, and (C) spherical ZnO/biochar samples.

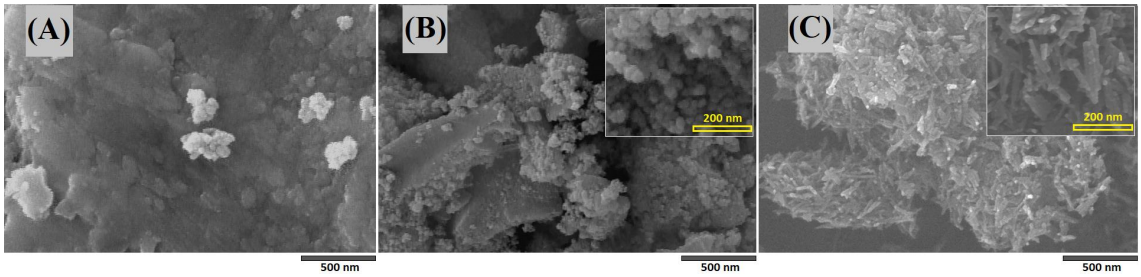

Fig. 3. SEM images of (A) biochar, (B) spherical ZnO/biochar catalyst, and (C) nanorod ZnO/biochar catalyst.

In the equation, C_0 (mg L^{-1}) and C_t (mg L^{-1}) represent the initial and final concentrations of the target dye. For the catalyst recycling experiments, the used ZnO/biochar was separated, completely washed with ethanol to remove the remaining impurities, and then dried at 50 °C. The experiments were carried out at least thrice.

RESULTS AND DISCUSSION

Characterization:

Fig. 1 illustrates the XRD patterns of the biochar and ZnO-biochar nanocomposites. No clear reflections of crystalline phases are observed in the XRD pattern of the biochar sample. However, there are two broad peaks at around 23.5° (002) and 43.5° (100), which are caused by graphitic carbon structures of support [32]. The various morphologies of the fabricated photocatalysts show similar XRD patterns. The peaks at 2θ values of 31.5°, 34.2°, 36.1°, 47.4°, 56.4°, 62.5°, 65.9°, and 67.5° could be indexed to (100), (002), (101), (102), (110), (103), and (112) crystal planes, respectively. The finding data are in agreement with the standard pattern of hexagonal ZnO (JCPDS No. 36-1451) [33, 34].

The FT-IR spectra of pistachio shells derived biochar and ZnO/biochar photocatalysts were investigated in the range of 400-4000 cm^{-1} and are depicted in Fig. 2. The presence of water molecules and surface hydroxyl groups can be identified by the broad band observed at ~3450 cm^{-1}. The bands observed at 2880 and 2939 cm^{-1} are a result of the C-H stretching vibrations in biochar material [35]. The presence of carboxylic groups of hemicellulose can be also identified by the adsorption band at 1635 cm^{-1} [36]. The peaks occurring at ~1070 cm^{-1} can be attributed to the stretching vibrations and anti-symmetric stretching of C-O-C bonds in biochar support [37]. The peaks at 516 and 491 cm^{-1} are due to the vibration of Zn-O bonds [38] and support the successful formation of ZnO particles on support material.

The SEM analyses of biochar and ZnO/biochar nanocomposites are demonstrated in Fig. 3. The biochar sample exhibits a relatively smooth surface, as shown in Fig. 3(A). The surface of the ZnO/biochar nanocomposites is rougher in comparison to biochar, suggesting that the ZnO particles have been covered on the carbon support. The successful deposition of ZnO on the biochar support resulted

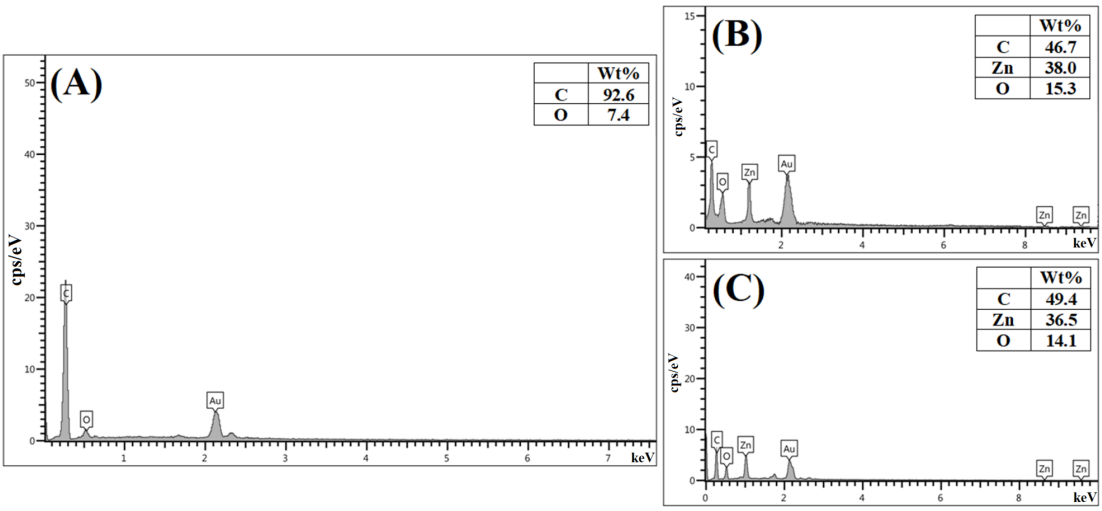

Fig. 4. EDS spectra of (A) biochar, (B) spherical ZnO/biochar catalyst, and (C) nanorod ZnO/biochar catalyst.

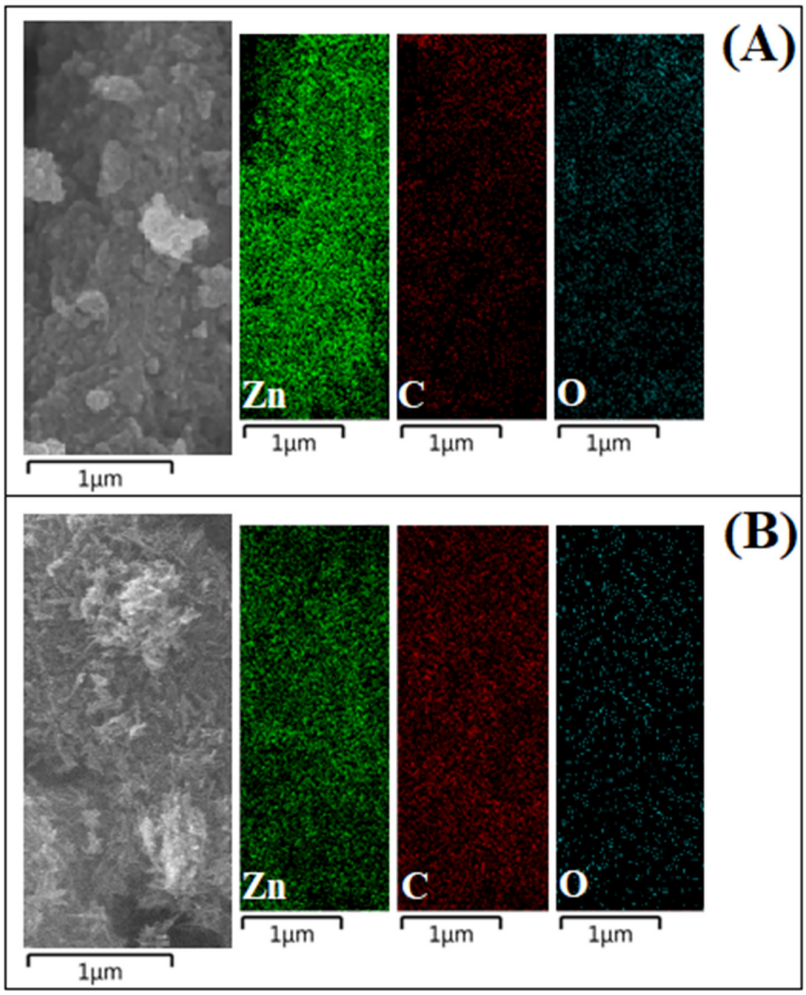

Fig. 5. EDS elemental mapping images of (A) spherical ZnO/biochar catalyst and (B) nanoroad ZnO/biochar catalyst.

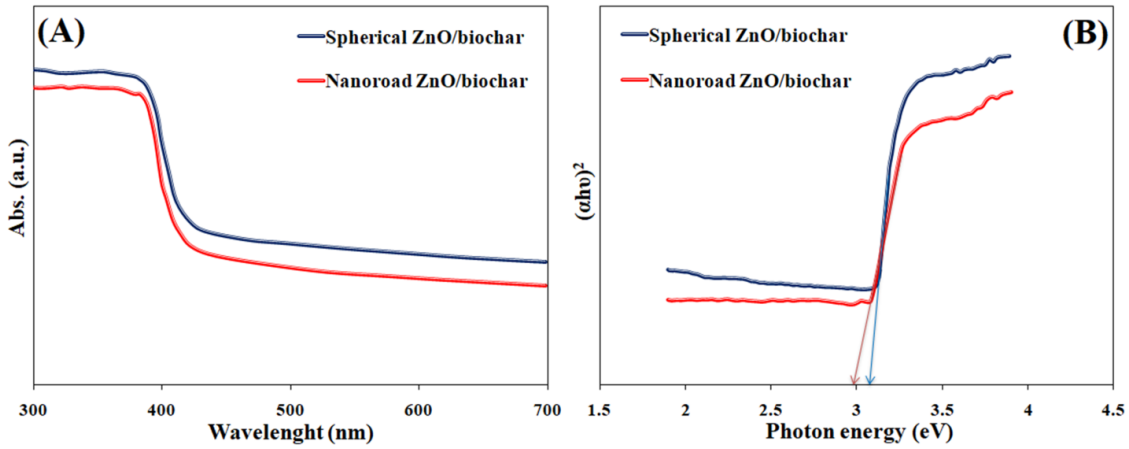

Fig. 6. (A) UV-vis diffuse reflectance spectra of ZnO/biochar catalysts and (B) corresponding relationship between $(\alpha h\upsilon)^2$ and photonic energy.

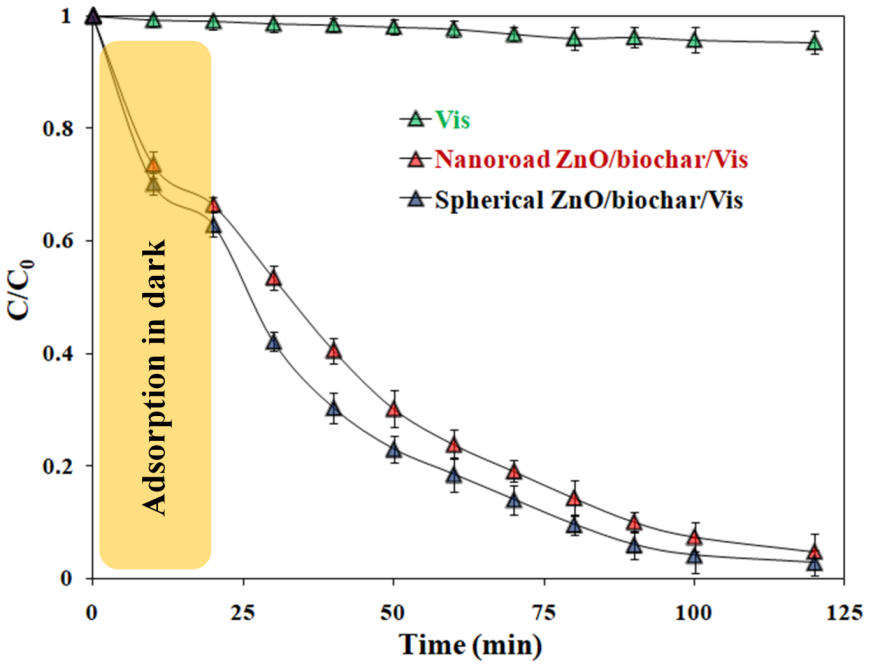

Fig. 7. Photodegradation studies of MB at different systems.

in the formation of various shapes, including spherical (Fig. 3(B)) and nanorod (Fig. 3(C)). To evaluate the chemical composition and elemental distribution, EDS analysis was performed. EDS analysis (Fig. 4) revealed that the ZnO/biochar nanocomposites consisted of zinc, oxygen, and carbon atoms, which confirm the successful preparation of photocatalysts. Fig. 5 presents the element mapping analyses of the spherical and nanorod ZnO/biochar materials. As can be seen, ZnO and C were uniformly distributed in both catalyst substances.

The optical characteristics of the spherical and nanorod ZnO/biochar materials were investigated by UV-vis DRS spectra as illustrated in Fig. 6(A). As depicted, both catalysts have strong absorption below 400 nm, which mainly corresponds to the intrinsic band absorption of ZnO [39]. The band-gap energies of the synthesized photocatalysts were determined using Tauc's plots using optical data.

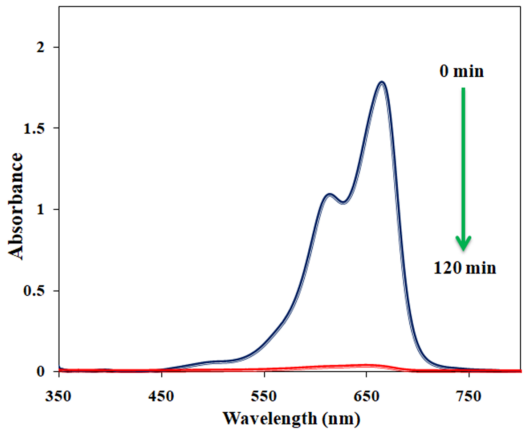

Fig. 8. UV-Vis spectra change of dye solution before and after 120 min treatment with spherical ZnO/biochar.

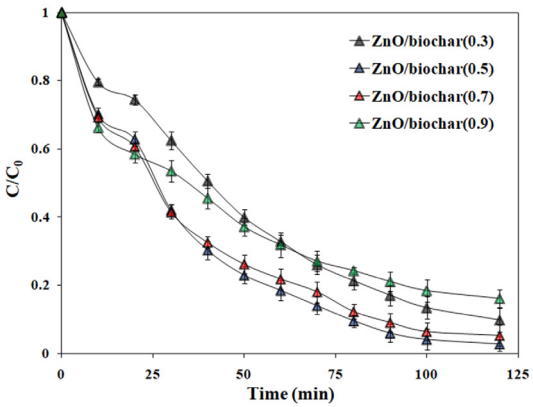

Fig. 9. Effect of biochar content on photodegradation of MB using spherical ZnO/biochar.

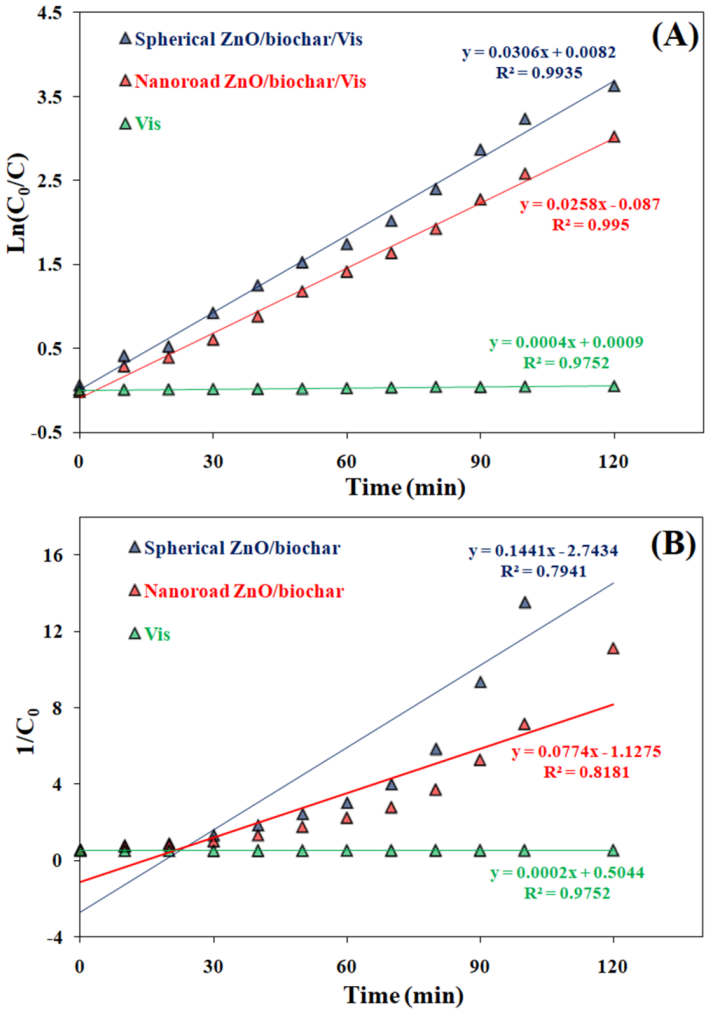

Fig. 10. Photodegradation kinetics with (A) pseudo-first-order and (B) pseudo-second-order models.

The band gap energies (Eg) were calculated using Tauc's equation [40]:

$$(\alpha h\nu)^2 = A\left(h\upsilon - E_g\right)$$

where α and A are the absorption coefficients, $h\upsilon$ and E_g are the photon energy and band gap energy, respectively. The band gap energy of the ZnO/biochar nanocomposites can be estimated by extrapolating the linear region of $(\alpha h\nu)^2$ versus $h\nu$ plot to zero absorption (Fig. 6(B)). The band gap values for spherical ZnO/biochar and nanoroad ZnO/biochar nanocomposites were determined to be 2.98 eV and 3.08 eV, respectively. Based on these results, the ZnO-based photocatalysts can demonstrate good visible photocatalytic character.

Photocatalytic activities:

Fig. 7 illustrates the degradation rate of MB when exposed to visible-light illumination in the presence of 10 mg of the synthesized spherical and nanorod ZnO/biochar catalysts. The nanorod ZnO/biochar showed a lower degradation rate compared to the spherical ZnO/biochar. The photodegradation performance of spherical and nanorod ZnO/biochar after 120 min visible-light irradiation was approximately ~97% and 95%, respectively. The concentration of dye showed little variation during visible-light irradiation without nanocatalysts, suggesting that the photolysis of MB is negligible. UV-Vis spectra of the dye solution before and after the photodegradation experiment using spherical ZnO/biochar are also shown in Fig. 8.

Effect of biochar content

Fig. 9 illustrates the performance profiles for the MB degradation using the spherical ZnO/biochar catalyst at various biochar contents (0.3, 0.5, 0.7, and 0.9 g). As depicted, the photocatalytic degradation efficiency of MB follows the order ZnO/biochar(0.5) > ZnO/biochar(0.7) > ZnO/biochar(0.3) > ZnO/biochar(0.9). The addition of an appropriate amount of biochar can enhance the photoactivity effectively. The excess amount addition of biochar content led to the reduction of the light penetration into the solution owing to the particle scattering effect [41, 42]. Hence, the ZnO/biochar (0.5) catalyst was used in further experiments.

Kinetic study:

The kinetics of the photodegradation process by the ZnO/biochar catalysts were investigated by the pseudo-first-order (Eq. 3) and pseudo-second-order (Eq. 4) kinetic models. These kinetic models are outlined as follows:

$$ln\frac{C_0}{C_t} = k_1 t \quad (3)$$

$$\frac{1}{C_t} - \frac{1}{C_0} = k_2 t \quad (4)$$

where, C_t (mg L^{-1}) is the dye concentration at time t, and C_0 (mg L^{-1}) is the initial dye concentration. The first-order and second-order equilibrium rate constants are denoted by k_1 (min^{-1}) and k_2 (g mg^{-1} min^{-1}), respectively. From Fig. 10, it is clear that the correlation coefficient (R^2) for the pseudo-first-order model is higher compared to the pseudo-second-order model. In addition, the rate constant (k_1) of 0.0306 min^{-1} and 0.0258 min^{-1} for the spherical ZnO/biochar and nanoroad ZnO/biochar catalysts was reckoned, respectively. This may be due to the existence of more oxygen vacancies and Zn centers in the spherical ZnO/biochar photocatalyst.

Reusability:

The study of catalyst reusability involved the repeated use of spherical ZnO/biochar for five cycles, with 120 min run time for each cycle. According to the data presented in Fig. 11, the efficiency loss for the first, second, third, fourth, and fifth cycles is 97.6%, 96.2%, 95.4%, 92.8%, and 90.8% respectively. Considering these results, the photodegradation treatment led to a slight decrease in the catalytic efficiency of the spherical ZnO/biochar. Therefore, the photodegradation of MB using the proposed nanocatalyst is economically feasible.

The performances of the spherical ZnO/biochar catalyst were also compared with other reported ZnO photocatalysts [33, 41, 43-45]. As summarized in Table 1, the suggested catalyst indicates the notable activity and stability for MB degradation under visible light irradiation. These data suggest that the spherical ZnO/biochar catalyst can be used as a promising photocatalyst material for water treatment. It is hoped that our current work could promote increasing interest in designing the nanocomposites of one-dimensional (1D) semiconductors and two-dimensional (2D) graphene for different photocatalytic applications.

Photocatalytic degradation mechanism:

The reactive species produced in the current

Table 1 Comparison of the performance of different ZnO-based photocatalysts for degradation of organic pollutants.

Catalyst	Target pollutant	Conditions	Efficiency (%)	Reusability (%)	Ref.
Graphene-ZnO nanorod	Methylene blue	[Catalyst]=0.21 g L^{-1}, [dye]=10 mg L^{-1}, UV irradiation (40 min)	>99	~95% (3rd)	[33]
ZnO/biochar composite	Metronidazole	[Catalyst]=0.2 g L^{-1}, [antibiotic]=10 mg L^{-1}, Visible-light (60 min)	97.5	80.1% (5th)	[41]
Nano-flower ZnO/biochar	Rhodamine B	[Catalyst]=1 g L^{-1}, [dye]=10 mg L^{-1}, Natural sunlight (120 min)	90	82.5% (3rd)	[43]
Activated carbon/ZnO	Congo red	[Catalyst]=1.25 g L^{-1}, [dye]=10 mg L^{-1}, Visible-light (50 min)	~100	-	[44]
Nano ZnO/Activated carbon	Methyl orange	[Catalyst]=0.2 g L^{-1}, [dye]=10 mg L^{-1}, UV irradiation (180 min)	>98	~83% (3rd)	[45]
Spherical ZnO/biochar	Methylene blue	[Catalyst]=0.2 g L^{-1}, [dye]=10 mg L^{-1}, Visible-light (120 min)	~97	90.8% (5th)	This study

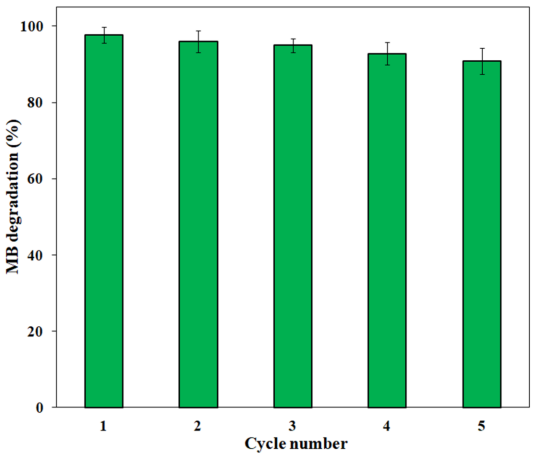

Fig. 11. Recycling experiments for MB photodegradation using spherical ZnO/biochar catalyst.

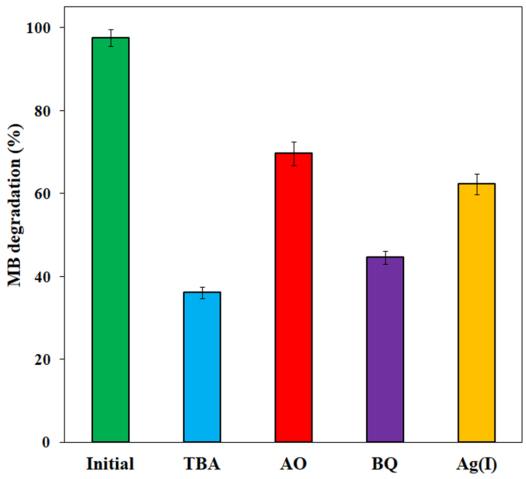

Fig. 12. Photocatalytic activity of spherical ZnO/biochar catalyst towards the degradation of MB with various types of scavengers.

photocatalytic method were identified by using *tert*-butyl alcohol (TBA), ammonium oxalate (AO), benzoquinone (BQ), and $AgNO_3$ for $OH^{\bullet}$, h^+, $O_2^{\bullet-}$ and e^-, respectively. As depicted in Fig. 12, when the TBA and AO are added, the photoactivity of spherical ZnO/biochar is lowered most significantly. The addition of $AgNO_3$ and BQ also prohibits the degradation performance but with a smaller depression degree for the photoactivity than the cases of TBA and AO added. These findings show that the $OH^{\bullet}$ and $O_2^{\bullet-}$radicals play a more important role than h^+ and e^- in the photocatalytic degradation of MB over spherical ZnO/biochar catalyst.

According to the above data, a possible mechanism for photocatalytic degradation of MB over spherical ZnO/biochar is proposed, as illustrated in Fig. 13. Upon the UV light irradiation, the electrons in the valence band of ZnO nanoparticles can be excited to the conduction band, leaving holes in the valence band. Then, the photogenerated electrons can transfer to biochar due to the interfacial contact between nanoparticles and biochar, which hinders the recombination of electrons and holes efficiently. The MB molecules can be transferred from the solution to the surface of the ZnO/biochar nanocomposite and adsorbed using π-π interaction between the target dye and

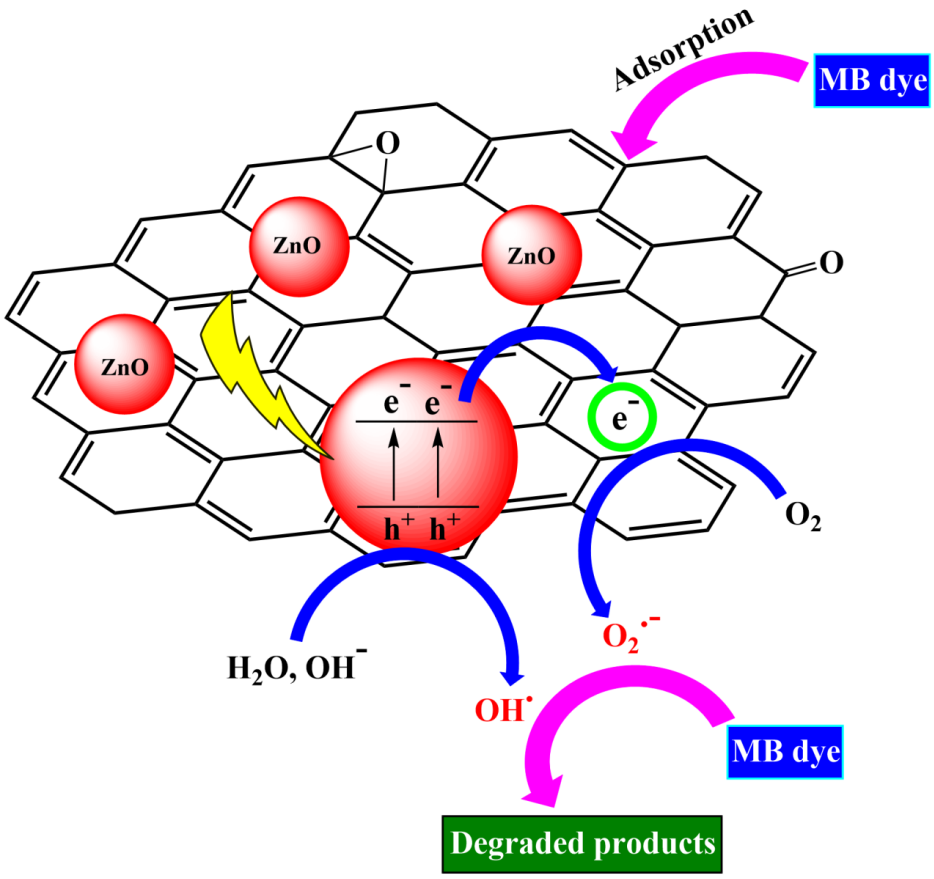

Fig. 13. Schematic diagram of the proposed mechanism for photodegradation of MB over spherical ZnO/biochar under visible light irradiation.

biochar surface. The adsorbed MB can be oxidized by the photoactive radicals (e.g., $OH^{\bullet}$ and $O_2^{\bullet-}$) generated in the photocatalytic reaction to produce CO_2, H_2O, and other mineralized intermediates. The photocatalytic reaction equations for the discussed mechanism are expressed in Eqs. (5)-(11).

$$ZnO/biochar + hv \rightarrow ZnO/biochar(h^+ + e^-) \quad (5)$$

$$2ZnO + hv \rightarrow ZnO(h^+) + ZnO(e^-) \quad (6)$$

$$ZnO(e^-) + biochar \rightarrow ZnO + biochar(e^-) \quad (7)$$

$$ZnO(h^+) + H_2O \rightarrow ZnO + OH^{\bullet} + H^+ \quad (8)$$

$$ZnO(h^+) + OH^- \rightarrow ZnO + OH^{\bullet} \quad (9)$$

$$biochar(e^-) + O_2 \rightarrow biochar + O_2^{\bullet-} \quad (10)$$

$$\text{Reactive species } (OH^{\bullet} \text{ and } O_2^{\bullet-}) + \text{MB} \rightarrow degraded\ products \quad (11)$$

CONCLUSION

In summary, ZnO nanostructures with different morphologies were successfully deposited on the surface of pistachio-derived biochar using the hydrothermal method and subsequent annealing treatment. XRD, SEM, DRS, and FTIR analyses were used to characterize the physicochemical features of the ZnO/biochar nanocatalysts. The SEM analysis shows that the deposited ZnO nanoparticles on carbon support have different morphologies (road and spherical). The photodegradation of MB at visible light conditions was examined to explore the catalytic properties of the fabricated ZnO-based photocatalyst materials. A photodegradation performance exceeding 97% was observed for the studied dye when treated with the ZnO/biochar photocatalysts. The notable photocatalytic ability of the as-prepared photocatalysts can be attributed to three key factors: the small size of ZnO nanoparticles, the adsorptive properties of the

carbon support, and the favorable separation of the photo-induced e-h pairs. Additionally, the ZnO/biochar photocatalysts offer several benefits, such as easy fabrication, cost-effectiveness, excellent photocatalytic performance, and effective recycling capability. These ZnO/biochar composites can be further explored for water purification at a larger and industrial scale.

CONFLICTS OF INTEREST

The authors declare that there are no conflicts of interest.

REFERENCES

[1] Musmade S, Hase DP, Waghmare AS, Kadam KR, Khedkar J, Gadhave AG, Bhavsar KS, Murade VD (2023) Synthesis of shape controlled Cu2O and Cu2O/TiO2-QD composite for degradation of Congo red dye under visible-light irradiation. Journal of Water and Environmental Nanotechnology 8(4):406-416. https://doi.org/10.22090/jwent.2023.04.007

[2] Sarmah P, Patir K, Gogoi SK (2023) Graphitic carbon nitride nanospheres as an adsorbent for effective waste water treatment: Methylene Blue removal from aqueous medium. Journal of Water and Environmental Nanotechnology 8(4):369-383. https://doi.org/10.22090/jwent.2023.04.004

[3] Gupta V (2009) Application of low-cost adsorbents for dye removal–a review. Journal of environmental management 90(8):2313-2342. https://doi.org/10.1016/j.jenvman.2008.11.017

[4] Rawat P, Nagarajan R (2018) Mechanochemical transformation of ZnO2 to highly defective ZnO. Materials Letters 212:178-181. https://doi.org/10.1016/j.matlet.2017.10.096

[5] MiarAlipour S, Friedmann D, Scott J, Amal R (2018) TiO2/porous adsorbents: Recent advances and novel applications. Journal of Hazardous materials 341:404-423. https://doi.org/10.1016/j.jhazmat.2017.07.070

[6] Trandafilović LV, Jovanović DJ, Zhang X, Ptasińska S, Dramićanin M (2017) Enhanced photocatalytic degradation of methylene blue and methyl orange by ZnO: Eu nanoparticles. Applied Catalysis B: Environmental 203:740-752. https://doi.org/10.1016/j.apcatb.2016.10.063

[7] Zheng H, Svengren H, Huang Z, Yang Z, Zou X, Johnsson M (2018) Hollow titania spheres loaded with noble metal nanoparticles for photocatalytic water oxidation. Microporous and Mesoporous Materials 264:147-150. https://doi.org/10.1016/j.micromeso.2018.01.012

[8] Zhang J, Zhang J (2013) A facile method for preparing a non-adhesive superhydrophobic ZnO nanorod surface. Materials Letters 93:386-389. https://doi.org/10.1016/j.matlet.2012.11.138

[9] Ehsani Amoli A, Masoomi M, Sharifzadeh Baei M, Babei F, Firouzzade Pasha G (2023) Visible light mediated photocatalytic anionic and cationic dyes degradation using ZnO-Fe2O3 nanocomposite. Journal of Water and Environmental Nanotechnology 8(1):52-65. https://doi.org/10.22090/jwent.2023.08.006

[10] Hong Y, Tian C, Jiang B, Wu A, Zhang Q, Tian G, Fu H (2013) Facile synthesis of sheet-like ZnO assembly composed of small ZnO particles for highly efficient photocatalysis. Journal of Materials Chemistry A 1(18):5700-5708. https://doi.org/10.1039/C3TA10218A

[11] Hosseinzadeh G (2023) Synthesis of novel pn heterojunction photocatalyst from ZnO nanorod and Cu2O nanoparticles for degradation of Paraoxon insecticide under visible light irradiation. Journal of Water and Environmental Nanotechnology 8(1):13-22. https://doi.org/10.22090/jwent.2023.08.002

[12] Barnes RJ, Molina R, Xu J, Dobson PJ, Thompson IP (2013) Comparison of TiO2 and ZnO nanoparticles for photocatalytic degradation of methylene blue and the correlated inactivation of gram-positive and gram-negative bacteria. Journal of nanoparticle research 15:1-11. https://doi.org/10.1007/s11051-013-1432-9

[13] Achouri F, Corbel S, Aboulaich A, Balan L, Ghrabi A, Said MB, Schneider R (2014) Aqueous synthesis and enhanced photocatalytic activity of ZnO/Fe2O3 heterostructures. Journal of Physics and Chemistry of Solids 75(10):1081-1087. https://doi.org/10.1016/j.jpcs.2014.05.013

[14] Fathi S, Aslibeiki B, Torkamani R (2023) Oxytetracycline photodegradation by transition metals doped ZnO nanorods. Journal of Water and Environmental Nanotechnology 8(3):254-266. https://doi.org/10.22090/jwent.2023.03.005

[15] Meena PL, Surela AK, Poswal K (2021) Fabrication of ZnO/CuO hybrid nanocomposite for photocatalytic degradation of brilliant cresyl blue (BCB) dye in aqueous solutions. Journal of Water and Environmental Nanotechnology 6(3):196-211. https://doi.org/10.22090/jwent.2021.03.001

[16] Okuda M, Tsuruta T, Katayama K (2009) Lifetime and diffusion coefficient of active oxygen species generated in TiO2 sol solutions. Physical Chemistry Chemical Physics 11(13):2287-2292. 11(13):2287-2292. https://doi.org/10.1039/B817695G

[17] Hakimi B, Ghorbanpour M, Feizi A (2018) A comparative study between photocatalytic activity of ZnO/bentonite composites prepared by precipitation, liquid-state ion exchange and solid-state ion exchange methods. Journal of Water and Environmental Nanotechnology 3(3):273-278. https://doi.org/10.22090/jwent.2018.03.008

[18] Brunet L, Lyon DY, Hotze EM, Alvarez PJ, Wiesner MR (2009) Comparative photoactivity and antibacterial properties of C60 fullerenes and titanium dioxide nanoparticles. Environmental science & technology 43(12):4355-4360. https://doi.org/10.1021/es803093t

[19] Das D, Nandi P (2021) Synthesis of CdS/GO modified ZnO heterostructure for visible light dye degradation applications. Applied Surface Science 570:151260. https://doi.org/10.1016/j.apsusc.2021.151260

[20] Ayon SA, Billah MM, Nishat SS, Kabir A (2021) Enhanced photocatalytic activity of Ho3+ doped ZnO NPs synthesized by modified sol-gel method: an experimental and theoretical investigation. Journal of Alloys and Compounds 856:158217. https://doi.org/10.1016/j.jallcom.2020.158217

[21] Stalin SS, Kirupa Vasam Jino E (2023) Fabrication of Cu doped ZnO nanocrystals hybridised with Graphene oxide nanosheets as an efficient solar light driven photocatalyst for the degradation of Quinalphos pesticide in aqueous medium. Journal of Water and Environmental Nanotechnology 8(2):94-107. https://doi.org/10.22090/jwent.2023.02.001

[22] Sanakousar F, Vidyasagar C, Jiménez-Pérez V, Prakash K

(2022) Recent progress on visible-light-driven metal and non-metal doped ZnO nanostructures for photocatalytic degradation of organic pollutants. Materials Science in Semiconductor Processing 140:106390. https://doi.org/10.1016/j.mssp.2021.106390

[23] Samadi M, Zirak M, Naseri A, Khorashadizade E, Moshfegh AZ (2016) Recent progress on doped ZnO nanostructures for visible-light photocatalysis. Thin solid films 605:2-19. https://doi.org/10.1016/j.tsf.2015.12.064

[24] Zhang B, Yang D, Qian Y, Pang Y, Li Q, Qiu X (2020) Engineering a lignin-based hollow carbon with opening structure for highly improving the photocatalytic activity and recyclability of ZnO. Industrial Crops and Products 155:112773. https://doi.org/10.1016/j.indcrop.2020.112773

[25] Tian N, Madani Z, Giannakis S, Isari AA, Arjmand M, Hasanvandian F, Noorisepehr M, Kakavandi B (2023) Peroxymonosulfate assisted pesticide breakdown: Unveiling the potential of a novel S-scheme ZnO@CoFe2O4 photocatalyst, anchored on activated carbon. Environmental pollution 334:122059. https://doi.org/10.1016/j.envpol.2023.122059

[26] Li X, Wang C, Zhang J, Liu J, Liu B, Chen G (2020) Preparation and application of magnetic biochar in water treatment: A critical review. Science of the total environment 711:134847. https://doi.org/10.1016/j.scitotenv.2019.134847

[27] Loo WW, Pang YL, Lim S, Wong KH, Lai CW, Abdullah AZ (2021) Enhancement of photocatalytic degradation of Malachite Green using iron doped titanium dioxide loaded on oil palm empty fruit bunch-derived activated carbon. Chemosphere 272:129588. https://doi.org/10.1016/j.chemosphere.2021.129588

[28] Saghir S, Pu C, Fu E, Wang Y, Xiao Z (2022) Synthesis of high surface area porous biochar obtained from pistachio shells for the efficient adsorption of organic dyes from polluted water. Surfaces and Interfaces 34:102357. https://doi.org/10.1016/j.surfin.2022.102357

[29] Kumaresan N, Ramamurthi K, Babu RR, Sethuraman K, Babu SM (2017) Hydrothermally grown ZnO nanoparticles for effective photocatalytic activity. Applied Surface Science 418:138-146. https://doi.org/10.1016/j.apsusc.2016.12.231

[30] Wahab R, Ansari S, Kim YS, Song M, Shin H-S (2009) The role of pH variation on the growth of zinc oxide nanostructures. Applied Surface Science 255(9):4891-4896. https://doi.org/10.1016/j.apsusc.2008.12.037

[31] Farazmand S, Fayazi M (2023) Single-step solvothermal synthesis of sepiolite-CoFe2O4 nanocomposite as a highly efficient heterogeneous catalyst for photo Fenton-like reaction. Materials Chemistry and Physics:128627. https://doi.org/10.1016/j.matchemphys.2023.128627

[32] Fayazi M, Ghanei-Motlagh M (2021) Enhanced performance of adsorptive removal of dibenzothiophene from model fuel over copper (II)-alginate beads containing polyethyleneterephthalate derived activated carbon. Journal of Colloid and Interface Science 604:517-525. https://doi.org/10.1016/j.jcis.2021.07.035

[33] Chen Z, Zhang N, Xu Y-J (2013) Synthesis of graphene–ZnO nanorod nanocomposites with improved photoactivity and anti-photocorrosion. CrystEngComm 15(15):3022-3030. https://doi.org/10.1039/C3CE27021A

[34] Fang L, Zhang B, Li W, Li X, Xin T, Zhang Q (2014) Controllable synthesis of ZnO hierarchical architectures and their photocatalytic property. Superlattices and Microstructures 75:324-333. https://doi.org/10.1016/j.spmi.2014.03.001

[35] Fayazi M, Ghanei-Motlagh M, Taher MA (2015) The adsorption of basic dye (Alizarin red S) from aqueous solution onto activated carbon/γ-Fe2O3 nano-composite: kinetic and equilibrium studies. Materials Science in Semiconductor Processing 40:35-43. https://doi.org/10.1016/j.mssp.2015.06.044

[36] Reddy KO, Maheswari CU, Dhlamini M, Mothudi B, Kommula V, Zhang J, Zhang J, Rajulu AV (2018) Extraction and characterization of cellulose single fibers from native african napier grass. Carbohydrate polymers 188:85-91. https://doi.org/10.1016/j.carbpol.2018.01.110

[37] Vinayagam M, Ramachandran S, Ramya V, Sivasamy A (2018) Photocatalytic degradation of orange G dye using ZnO/biomass activated carbon nanocomposite. Journal of Environmental Chemical Engineering 6(3):3726-3734. https://doi.org/10.1016/j.jece.2017.06.005

[38] Mahalakshmi S, Hema N, Vijaya PP (2020) In vitro biocompatibility and antimicrobial activities of zinc oxide nanoparticles (ZnO NPs) prepared by chemical and green synthetic route—a comparative study. BioNanoScience 10(1):112-121. https://doi.org/10.1007/s12668-019-00698-w

[39] Ding C, Fu K, Pan Y, Liu J, Deng H, Shi J (2020) Comparison of Ag and Agi-modified zno as heterogeneous photocatalysts for simulated sunlight driven photodegradation of metronidazole. Catalysts 10(9):1097. https://doi.org/10.3390/catal10091097

[40] Firat Y, Peksoz A (2019) Efficiency enhancement of electrochromic performance in NiO thin film via Cu doping for energy-saving potential. Electrochimica Acta 295:645-654. https://doi.org/10.1016/j.electacta.2018.10.166

[41] Cai H, Zhang D, Ma X, Ma Z (2022) A novel ZnO/biochar composite catalysts for visible light degradation of metronidazole. Separation and Purification Technology 288:120633. https://doi.org/10.1016/j.seppur.2022.120633

[42] Isari AA, Payan A, Fattahi M, Jorfi S, Kakavandi B (2018) Photocatalytic degradation of rhodamine B and real textile wastewater using Fe-doped TiO2 anchored on reduced graphene oxide (Fe-TiO2/rGO): Characterization and feasibility, mechanism and pathway studies. Applied Surface Science 462:549-564. https://doi.org/10.1016/j.apsusc.2018.08.133

[43] Kaur H (2022) Synergistic effect of biochar impregnated with ZnO nano-flowers for effective removal of organic pollutants from wastewater. Applied Surface Science Advances 12:100339. https://doi.org/10.1016/j.apsadv.2022.100339

[44] Loo WW, Pang YL, Wong KH, Lim S, Mah SK, editors. Adsorption-photocatalysis of organic dyes using empty fruit bunch activated carbon-metal oxide photocatalyst. IOP Conference Series: Materials Science and Engineering; 2018. IOP Publishing. https://doi.org/10.1088/1755-1315/1135/1/012005

[45] Nasrollahzadeh MS, Hadavifar M, Ghasemi SS, Arab Chamjangali M (2018) Synthesis of ZnO nanostructure using activated carbon for photocatalytic degradation of methyl orange from aqueous solutions. Applied Water Science 8:1-12. https://doi.org/10.1007/s13201-018-0750-6